Rescue by 4-phenylbutyrate of several misfolded creatine transporter-1 variants linked to the creatine transporter deficiency syndrome

Ali El-Kasaby[a,1], Ameya Kasture[a,b,1], Florian Koban[a], Matej Hotka[c], Hafiz M.M. Asjad[a,d], Helmut Kubista[c], Michael Freissmuth[a], Sonja Sucic[a,*]

[a] *Institute of Pharmacology and the Gaston H. Glock Research Laboratories for Exploratory Drug Development, Center of Physiology and Pharmacology, Medical University of Vienna, Austria*
[b] *Department of Neurobiology, University of Vienna, Austria*
[c] *Department of Neurophysiology and Neuropharmacology, Center of Physiology and Pharmacology, Medical University of Vienna, Austria*
[d] *Department of Pharmacy, Forman Christian College, Lahore, Pakistan*

HIGHLIGHTS

- Genetic mutations in CRT-1 cause the creatine transporter deficiency (CTD) syndrome.
- CTD variants trigger protein misfolding, trapping the transporter in the ER.
- Several mutants are amenable to functional rescue by 4-phenyl butyrate.

ARTICLE INFO

ABSTRACT

Diseases arising from misfolding of SLC6 transporters have been reported over recent years, *e.g.* folding-deficient mutants of the dopamine transporter and of the glycine transporter-2 cause infantile/juvenile Parkinsonism dystonia and hyperekplexia, respectively. Mutations in the coding sequence of the human creatine transporter-1 (hCRT-1/SLC6A8) gene result in a creatine transporter deficiency syndrome, which varies in its clinical manifestation from epilepsy, mental retardation, autism, development delay and motor dysfunction to gastrointestinal symptoms. Some of the mutations in hCRT-1 occur at residues, which are highly conserved across the SLC6 family. Here, we examined 16 clinically relevant hCRT-1 variants to verify the conjecture that they were misfolded and that this folding defect was amenable to correction. Confocal microscopy imaging revealed that the heterologously expressed YFP-tagged mutant CRTs were trapped in the endoplasmic reticulum (ER), co-localised with the ER-resident chaperone calnexin. In contrast, the wild type hCRT-1 reached the plasma membrane. Preincubation of transiently transfected HEK293 cells with the chemical chaperone 4-phenylbutyrate (4-PBA) restored ER export as well as substrate uptake by several folding-deficient CRT-1 mutants. A representative mutant (hCRT-1-P544L) was expressed in rat primary hippocampal neurons to verify pharmacochaperoning in a target cell: 4-PBA promoted the delivery of hCRT-1-P544L to the neurite extensions. These observations show that several folding-deficient hCRT-1 mutants can be rescued. This proof-of-principle justifies the search for additional pharmacochaperones to restore folding of 4PBA-unresponsive hCRT-1 mutants. Finally, 4-PBA is an approved drug in paediatric use: this provides a rationale for translating the current insights into clinical trials.

This article is part of the issue entitled 'Special Issue on Neurotransmitter Transporters'.

1. Introduction

The human creatine transporter 1 (hCRT-1, SLC6A8) belongs to the sodium dependent neurotransmitter family of solute carrier 6 (SLC6) transporters. It is a protein of 635 amino acid residues, organised into twelve transmembrane spanning helices (TM1-TM12). Over the past

decade, a number of studies reported point mutations in the hCRT-1 protein; these have been associated with the X-linked cerebral creatine deficiency syndrome resulting from a loss of function of CRT-1: the creatine transporter deficiency syndrome affects the brain, skeletal muscle and other organs to a variable degree. Symptoms range from epilepsy, moderate to severe mental retardation, autism, development delay (in walking and speech), abnormal behaviour (attention deficit hyperactivity disorder/ADHD, shyness, aggression, self-injury) and motor dysfunction (stiff gait, coordination dysfunction and dystonia) to gastrointestinal symptoms (neonatal feeding difficulties, vomiting, constipation, ulcers) (Hahn, 2002; Rosenberg et al., 2004; Lion Francois et al., 2006; van de Kamp et al., 2013; Ardon et al., 2016; Uemura et al., 2017; Heussinger et al., 2017). Based on a study of 188 consecutive mentally retarded children, the prevalence of creatine transporter deficiency was estimated to be 2.7% (Lion-François et al., 2006). However, this percentage rises to 4.4%, if only boys are taken into account. The ratio of 2.7%–4.4% shows that girls are also affected in spite of the X-linked nature of genetic transmission. In the presence of mutations, all males and about 50% of the affected females display intellectual and cognitive dysfunction (DesRoches et al., 2015). The nature of the mutation is an important determinant for the phenotypic consequence. In fact, only mild neuropsychological impairments were observed in several cases, where female relatives were heterozygous for mutations, *e.g.* for the G381R and R514X variants (Lion-François et al., 2006). The estimated carrier prevalence of CTD in females in the general population is at least 0.024% (DesRoches et al., 2015). The true prevalence of creatine transporter deficiency may be underrated; the reason for this being either misdiagnosis or underdiagnosis, as most CTD patients are diagnosed with other neurological disorders such as autism, ADHD, or unexplained mental retardation.

Apart from a few mutations, which affect intracellular and extracellular loops of hCRT-1, the mutations are primarily found in the hydrophobic core of the transporter; in fact, TMDs 7 and 8 appear to be a hot spot for mutations (Freissmuth et al., 2018). Several mutations are found at positions, which are conserved in SLC6 transporters, *e.g.* a single point mutation in TM3, which induces a sleepless phenotype in the Drosophila dopamine (dDAT-G108Q) (Kasture et al., 2016), leads to severe mental retardation in children when mutated at the equivalent glycine residue in hCRT-1 (hCRT-1-G132V) (Lion-François et al., 2006). Similarly, the P554L mutation causes Parkinsonism/dystonia in hDAT and triggers drug-resistant epilepsy in children harbouring the same mutation in CRT-1. Currently, there is no effective treatment for patients suffering from creatine transporter deficiency: the current standard therapy relies on supplementation of creatine monohydrate, L-arginine and glycine, but a long-term study of children only showed that short term benefits did not translate into a sustained improvement (van de Kamp et al., 2012); the symptoms substantially deteriorated in those patients who survived into adulthood. This unmet medical need justifies the search for effective therapeutic strategies in the treatment of creatine transporter deficiency. In the present study, we explored the hypothesis that many of the mutations, which trigger creatine transporter deficiency, result in misfolding of hCRT-1 and that this folding deficiency can be corrected by pharmacological means.

2. Material and methods

2.1. Chemicals

[³H]Creatine (creatine [N-methyl-³H], specific activity 70–80 Ci/mmol) was obtained from ARC (American Radiolabelled Chemicals). Cell culture media, supplements, and antibiotics were purchased from Invitrogen. Other cell culture reagents, such as BSA and Complete™ protease inhibitor mixture, were purchased from Roche Applied Science, SDS from BioMol (Hamburg, Germany), scintillation mixture (Rotiszint® eco plus), and Tris from Carl Roth (Karlsruhe, Germany). The rabbit polyclonal anti-GFP antibody (ab290) was obtained from
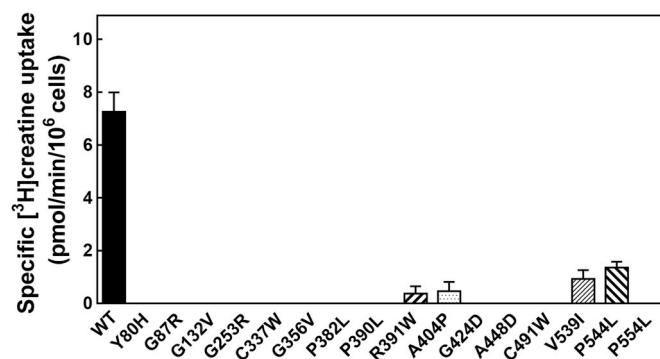

Fig. 1. Lack of substrate transport by HEK293 cells expressing hCRT-1 variants associated with CTD. HEK293 cells expressing wild-type hCRT-1 and 16 CTD-triggering mutants thereof were seeded onto poly-D-lysine coated 48-well plates 24 h after the transfections. Specific [³H]creatine uptake was determined after an additional 24 h by incubating the cells with 10 nM [³H] creatine, which was diluted with unlabeled creatine (up to a final concentration of 1 μM). Non-specific uptake was calculated by subtracting the uptake measure in non-transfected cells in Krebs-HEPES/LiCl buffer, as described under *Material and Methods*. The data were obtained from four independent experiments, performed in triplicate. The creatine uptake by all 16 mutants was either abolished or significantly reduced compared to the wild type transporter (one-way ANOVA followed by *post hoc t* tests: P < 0.05).

Abcam (Cambridge, UK). Protein A-sepharose and horseradish peroxidase–linked anti-rabbit IgG1 antibody were purchased from Amersham Biosciences. All other chemicals used in experiments were of analytical grade. 4-Phenylbutyric acid (4-PBA) and the 0.4% trypan blue solution were both obtained from Sigma–Aldrich.

2.2. DNA constructs and cloning

The cDNA encoding the creatine transporter-1/SLC6A8 (transcript variant 1; SC116601, ORIGENE) was amplified by PCR and inserted into the YFP-N1 vector (Clontech, Mountainview, CA) *via* the restriction sites for Eco RI (R3101S, NEB) and Hind III (R3104S, NEB). The mutants were created with the QuikChange Lightning Site-Directed Mutagenesis Kit (Stratagene, La Jolla, CA), using the wild type hCRT-1 as template. All mutations were confirmed by automatic DNA sequencing (LGC Labor GmbH Augsburg, Germany).

2.3. Cell culture and transfections

HEK293 cells were cultured in Dulbecco's modified Eagle's medium (DMEM) with high glucose (4.5 g/liter) and l-glutamine (584 mg/L), supplemented with 10% fetal calf serum (FCS). Transfections were done using Lipofectamine 2000 Reagent (Life Technologies, Carlsbad, CA) for uptake experiments or jetPRIME® (polyplus transfection™) for fluorescence microscopy experiments. Some of the experiments were also carried out in stable cell lines expressing the wild type hCRT-1 and the mutants of interest. In short, 10 cm dishes of 80% confluent HEK293 were transfected with YFP-CRT-WT, YFP-CRT-R391W, YFP-CRT-P544L (4 μg plasmid DNA and 12 μL Lipofectamine 2000) according to the protocol of the manufacturer. After 24 h, the cells were detached by trypsinisation and seeded onto 15 cm dishes. Geneticin (G418) was added to select for cells with genomic plasmid integration.

2.4. Creatine uptake assays

[³H]Creatine uptake was performed as described previously (Straumann et al., 2006) with some modifications: 24 h after transfection, HEK293 cells were seeded onto 48-well plates (6 × 10⁵/well) precoated with poly-D-lysine. The following day, the medium was removed, and cells were washed twice with 1 ml Hanks' Balanced Salt
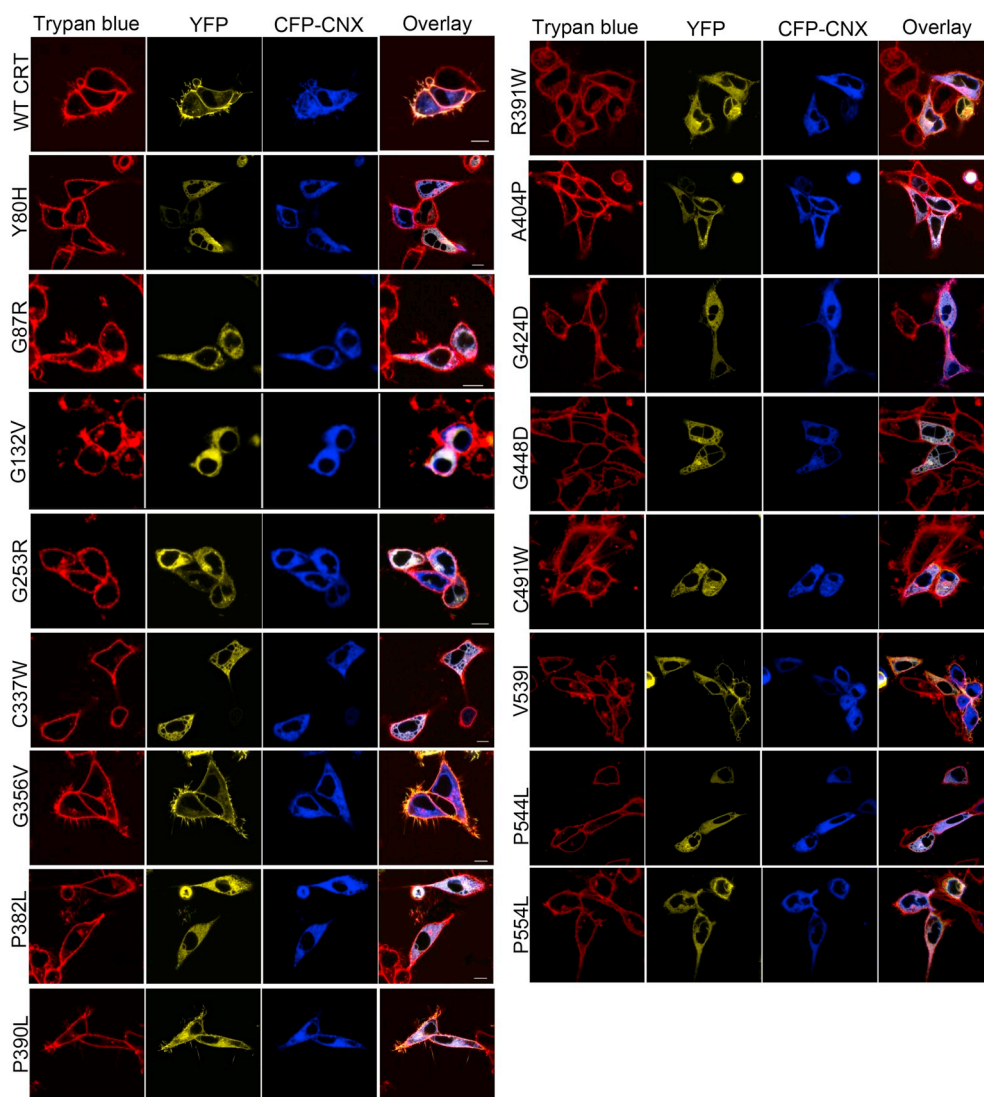
Fig. 2. Subcellular localization of CTD-causing hCRT-1 variants. HEK293 cells were transiently transfected with plasmids encoding hCRT-1-YFP and 16 mutants thereof (shown in yellow) and CFP-calnexin (CFP-CNX, shown in blue). After 24 h, the cells were seeded onto poly-D-lysine coated ibidi® glass bottom chambers and confocal microscopy performed the next day. Trypan blue (0.04% in PBS, shown in red) was used to delineate the plasma membrane. Co-localization of the three signals is shown in the overlay images. Pearson's coefficient values (described under *Material and Methods*) for co-localization of trypan blue and the YFP-tagged transporters were: 0.60 (CRT1-WT), -0.22 (Y80H), -0.14 (G87R), -0.08 (G132V), -0.06 (G257R), -0.22 (C337W), -0.04 (G356V), -0.2 (P382L), -0.15 (P390L), -0.02 (R391W), -0.11 (A404P), -0.15 (G424D), -0.17 (A448D), -0.16 (C491W), -0.22 (V539I), -0.12 (P544L) and -0.19 (P554L). (For interpretation of the references to colour in this figure legend, the reader is referred to the Web version of this article.)

Solution (Sigma 55037C) and serum-starved for 30 min at 37 °C in Hank's Balanced Salt Solution. The cells were then washed twice using Krebs-HEPES buffer (10 mM HEPES.NaOH, pH = 7.4, 4.7 mM KCl, 2.2 mM $CaCl_2$, 1.2 mM $MgSO_4$, 10 mM glucose, 120 mM NaCl). For uptake, the cells were incubated in uptake buffer containing 10 nM [^{3}H] creatine. For single concentration point uptake measurements, unlabeled creatine was added up to a total concentration of 1 μM. For saturation uptake kinetic assays, [^{3}H]creatine was diluted with increasing concentrations of unlabeled creatine in the range of 1–150 μM. After a 6 min incubation time, the cells were rapidly washed twice with 1 ml ice-cold Krebs-HEPES buffer, in which NaCl was replaced by LiCl (120 mM). Non-specific uptake was determined in parallel in both, untransfected and transfected HEK293 cells, in the presence of Krebs-HEPES-buffer containing 120 mM LiCl, which gave comparable results, and was subtracted from total uptake. Cells were lysed in 1% SDS, the lysates transferred to scintillation vials and the radioactivity content was determined by liquid scintillation counting.

2.5. Enzymatic deglycosylation and immunoblotting

After 24 h, transiently transfected HEK293 cells were split and incubated in the presence or absence of 4-PBA (5 mM). After another 24 h, cells were lysed in a buffer containing 50 mM Tris.HCl (pH 8.0), 150 mM NaCl, 1% dodecylmaltoside, 1 mM EDTA and protease inhibitors (Roche Complete™); the lysates were rotated at 4 °C for 1 h.

Insoluble material was removed by centrifugation (30 min at 13,000 g at 4 °C). Aliquots of the lysate (protein content 20 μg) were incubated in the absence and presence of PNGase F, O-glycosylation and endoglycosidase H and using the NEB assay kit according to the protocol of the manufacturer. Proteins (20 μg) were separated by denaturing polyacrylamide gel electrophoresis (resolving gel 7% monomer concentration) and transferred onto nitrocellulose membranes. These were first blocked with 3% bovine serum albumin in Tris-buffered saline containing 0.1% Tween 20 (TBST) and then a rabbit polyclonal antibody directed against GFP overnight at 4 °C. After repeated washes, the immunoreactivity was detected by chemoluminescence (Amersham ECL Prime Western Blotting Detection Reagent) using a horseradish peroxidase-(HRP)-conjugated secondary antibody (1:5000). Immunostaining with an antiserum, which recognizes all G protein β-subunits (Hohenegger et al., 1996), was used to verify comparable loading of individual lanes.

2.6. Laser scanning microscopy and image analysis

HEK293 cells expressing wild-type hCRT-1-YFP or mutants of interest were seeded onto 8-well ibidi® glass-bottomed μ-slides. The incubation with 4-PBA was done as described above (see 2.5.). Images were captured on a Zeiss LSM780 equipped with an argon laser (at 30 mW) and a 63 × oil immersion objective (Zeiss Plan-Neofluar). Trypan blue solution (0.05% in PBS) was used to stain the plasma
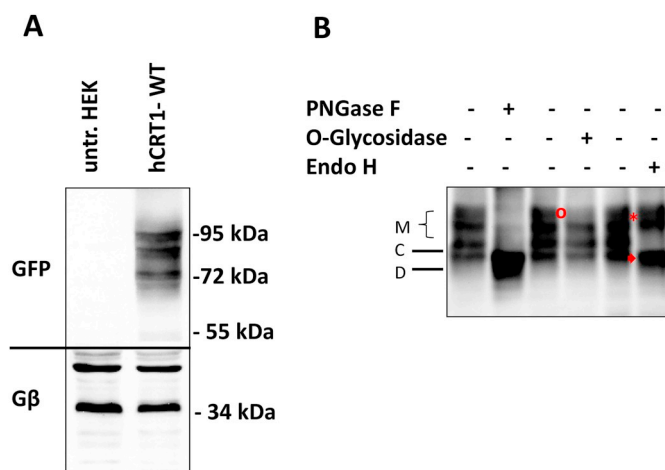
Fig. 3. Characterization of the C-terminally tagged hCRT-1 protein. (A) Detergent lysates were prepared from HEK293 cells, either untransfected (untr. HEK, left lane) or expressing the wild type hCRT-1 protein carrying a C-terminal YFP tag (hCRT-1 WT, right lane). Aliquots of the lysates (20 μg) were resolved by SDS-polyacrylamide gel electrophoresis. After transfer of the proteins to nitrocellulose, immunoreactive bands were visualized with an anti-GFP antibody. G protein β-subunits (Gβ) served as a loading control. (B) Aliquots of the WT hCRT-1-YFP lysates (20 μg) were incubated in the absence (lanes 1, 3 and 5) and presence of peptide-N-glycosidase F (PNGaseF, 1000 U, lane 2), O-glycosidase (160000 U, lane 4), endoglycosidase H (Endo H, 1500 U, lane 6) for 2 h at 37 °C prior to electrophoretic separation and transfer the nitrocellulose membrane. The immunoblot shows the deglycosylation pattern of the WT hCRT-1-YFP by the three enzymes. The red circle denotes the effect of O-glycosylation. The asterisk denotes the mature glycosylated upper band, which is Endo H-resistant (M); the lower core-glycosylated band (C), is cleaved by Endo H to generate a smaller product (marked with *red arrow*, D). The immunoblots shown are representative of three independent experiments. (For interpretation of the references to colour in this figure legend, the reader is referred to the web version of this article.)

membranes, as described previously (Sucic et al., 2010). The images were analysed using Image J. ImarisColoc function of Bitplane Imaris 9.2 software was used to measure the Pearson's coefficient. The software utilises the algorithms of Costes et al. (2004) in the analysis of Pearson's coefficient. Values of 1 and -1 represent 100% co-localization and an inverse distribution, respectively.

2.7. Preparation of hippocampal neuronal cultures, transfection, confocal microscopy and image analysis

As described in Geier et al. (2011), hippocampi from neonatal Sprague–Dawley rats were dissected to prepare primary cultures of hippocampal neurones, which were seeded onto 3.5 cm glass bottom cell culture dishes. DMEM high glucose with l-glutamine (PAA, Pasching, Austria) supplemented with 10% heat-inactivated foetal calf serum (Invitrogen, Lofer, Austria) was used as a culture medium. Neurones were cultured at 37 °C and 5% CO_2. One-week-old neurons were transfected with plasmids (1 μg) encoding WT hCRT1-YFP and hCRT1-P544L-YFP using Lipofectamine 2000 (3 μl in 0.5 ml) according to the manufacturer's protocol. After 24 h, neurones were incubated in the presence of 4-PBA for transfection for an additional 24 h period. Thereafter, neurones were fixed in 3.7% paraformaldehyde in PBS for 20 min at room temperature. Images were captured by confocal microscopy under oil immersion (63x objective, numerical aperture 1.4) with a Zeiss LSM780 confocal microscope. Images were analysed using the Image J software. The Sholl analysis plugin was used to measure the distribution of hCRT-1-YFP and –P544L mutant across the neurites, with radii increasing in 2 μm increments. The distribution of wild type and mutant CRT-1 was quantified by calculating the area under the curve (AUC) for the different conditions. The Kruskal-Wallis test

followed by Dunn's multiple comparison was used to calculate statistical differences in the distribution pattern of wild type and mutant hCRT-1.

3. Results

3.1. Naturally occurring variants of hCRT-1 trigger disease due to protein misfolding

All constructs were tagged with yellow fluorescent protein (YFP) to examine their subcellular distribution. We verified that this C-terminal tag did not impair the kinetics of transport: substrate uptake of tagged and untagged hCRT-1 were comparable (data not shown). We selected sixteen naturally occurring variants of the hCRT-1, which had been identified in children suffering from the creatine transporter deficiency (CTD) syndrome, primarily manifested by mental retardation in the afflicted patients. The mutations are scattered throughout the hCRT-1 protein, both in the transmembrane and loop regions of the transporter (for the homology model, see Freissmuth et al., 2018). When heterologously expressed in HEK293 cells, all hCRT-1 variants proved to be loss-of-function mutants (Fig. 1): the majority of the mutants did not support any appreciable creatine uptake; however, in several of the mutants (*i.e.* R391W, A404P, V539I and P544L), creatine uptake reached some 10–20% of wild type uptake levels (Fig. 1). Abolition of uptake can have many causes, *e.g.* a mutation may trap the transporter in a conformational state and thus block progression through the transport cycle and/or impair trafficking/surface expression of the transporter and/or result in the loss of affinity for the endogenous substrate creatine. For the 16 hCRT-1 mutants examined here, we found that the functional deficit was due to their absence at the plasma membrane: confocal laser scanning microscopy of C-terminally YFP-tagged hCRT-1 mutants revealed that most mutations led to the entrapment of the protein within the cell (Fig. 2): their distribution was superimposed with that of calnexin, an endoplasmic reticulum (ER)-resident chaperone. In contrast, the wild type hCRT-1 was targeted to the cell surface and co-localised with trypan blue (the Pearson coefficient for WT hCRT-1-YFP was 0.6, and was negative for all the mutants), which was used to delineate the plasma membranes (Fig. 2, left hand top row).

3.2. The response of hCRT-1 mutants to small molecules

The retention of the hCRT-1 mutants in the ER is indicative of their misfolding. Folding deficiencies can be corrected by chemical and pharmacological chaperones, which facilitate folding and/or the escape of mutant proteins from the ER quality control machinery and thus allow for their delivery to the correct subcellular location (Kasture et al., 2017). The relative proportion of protein, which is retained in the ER, can be assessed by examining the pattern of glycosylation: ER-resident membrane proteins are core-glycosylated; N-linked core glycans are cleaved by both, endoglycosidase H and peptide:N-glycosidase F (PNGase F). Membrane proteins, which have been exported from the ER and which have reached the Golgi apparatus, acquire mature N-linked glycans. We relied on the YFP-tag to detect hCRT-1; untransfected HEK 293 cells were devoid of any immunoreactivity (left-hand lane in Fig. 3A). The fluorescent tag adds a mass of about 27 kDa to the fusion protein, which was detected as a collection of bands in the range of 70–100 kDa (right-hand lane in Fig. 3A). The heterogeneity of hCRT-1 is due to the presence of multiple glycosylation sizes; there are three putative N-linked glycosylation sites, two in extracellular loop-2 (Asn^{192}, Asn^{197}) and one in extracellular loop-6 (Asn^{548}) (Christie, 2007). Digestion by PNGAse F removed most of the heterogeneity (second lane in Fig. 3B). In contrast, Endo H only cleaved the lower bands, the mobility of the upper bands was not affected (last lane in Fig. 3B). We noted that treatment with PNGase F did not eliminate all heterogeneity, i.e. the band (labelled D in Fig. 3B) was still broad.
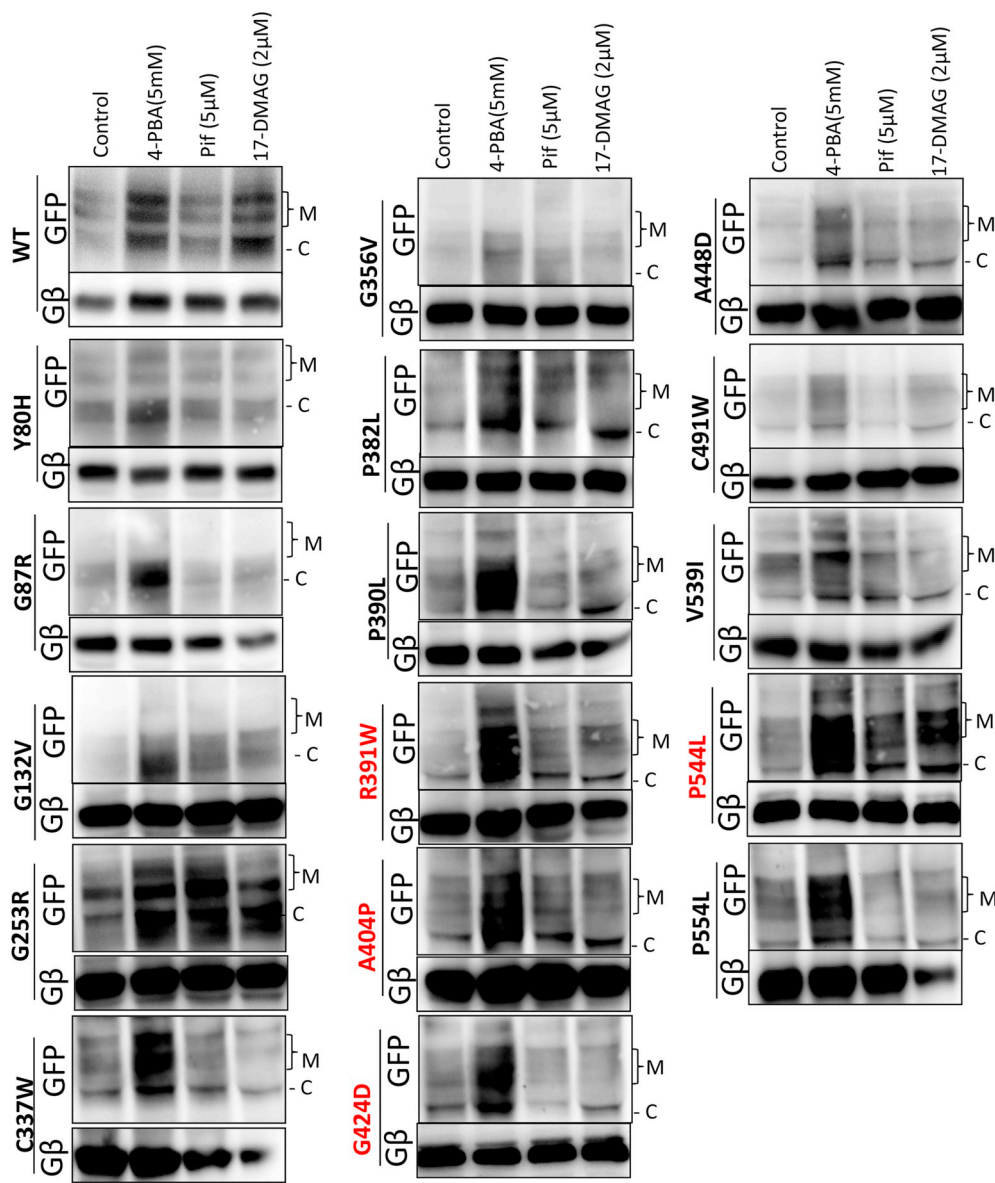
Fig. 4. A screen of small molecules for their capacity to restore mature glycosylation of CTD-causing hCRT-1 mutants. Detergent lysates were prepared from HEK293 cells expressing the WT hCRT-1-YFP and CTD variants, which had been incubated in the absence and presence of 4-PBA (5 mM), pifithrin-μ (5 μM) or 17-DMAG (2 μM) for 24 h. Aliquots of the lysates (20 μg) were resolved by SDS-polyacrylamide gel electrophoresis. After transfer of the proteins to nitrocellulose, immunoreactive bands were visualized with an anti-GFP antibody. G protein β-subunits (Gβ) served as a loading control.

Accordingly, we searched for possible additional modifications: three O-linked glycosylation sites were predicted by NetOglyc software (Steentoft et al. 2013) in the second extracellular loop (EL2) of hCRT-1: Thr^{171}, Thr^{175} and Thr^{178} with scores of 0.61, 0.63 and 0.57, respectively. Exposure of the detergent extract to O-glycosidase accelerated the migration of some species of hCRT-1 such that the upper most bands were removed (lane 4 in Fig. 3B, bands labelled by a red circle). Based on the susceptibility to enzymatic digestion, we conclude that the upper and the lower bands represent the mature glycosylated species (labelled M in Fig. 3B) and the ER-resident core-glycosylated protein (labelled C in Fig. 3B), respectively.

We tested the response of hCRT-1 mutants to the chemical chaperone 4-phenyl butyrate (4-PBA) and the inhibitors of heat shock proteins (HSP) pifithrin-μ and 17-DMAG. Upon incubation of cells with 4-PBA (5 mM), HSP70 blocker pifithrin-μ (5 μM) or HSP90 blocker 17-DMAG (2 μM), we observed increases in total protein expression of most variants of hCRT-1 examined. The quantification indicated that there was a robust and statistically significant increase in the mature glycosylated bands of 6 mutants - i.e., hCRT-1-R391W, -A404P, -G424D, -V539I, -P544L and -P554L (see bar graphs in Fig. 4) - upon treatment with 5 mM 4-PBA. The effects produced by either pifithrin-μ or 17-DMAG were not as pronounced as those achieved by 4-PBA (Fig. 4).

3.3. Treatment with 4-PBA restores the activity of several CTD-inducing variants, R391W, A404P, G424D, V539I and P544L

Transporters can only take up the substrate, if they reach the plasma membrane. The preincubation with 5 mM 4-PBA also restored substrate transport by these six CTD-triggering variants, namely hCRT-1-R391W, -A404P, -G424D, -V539I, -P544L and -P554L (Fig. 5), which had been identified based on their glycosylation pattern (Fig. 4). Several mutants were responsive to 4-PBA. For further characterization, we selected one mutation from an extracellular loop (R391W in EL4), two mutations (A404P and G424D) from TM8 (a helix, which is a hot spot for mutations and which is though to line the translocation pathway) and one
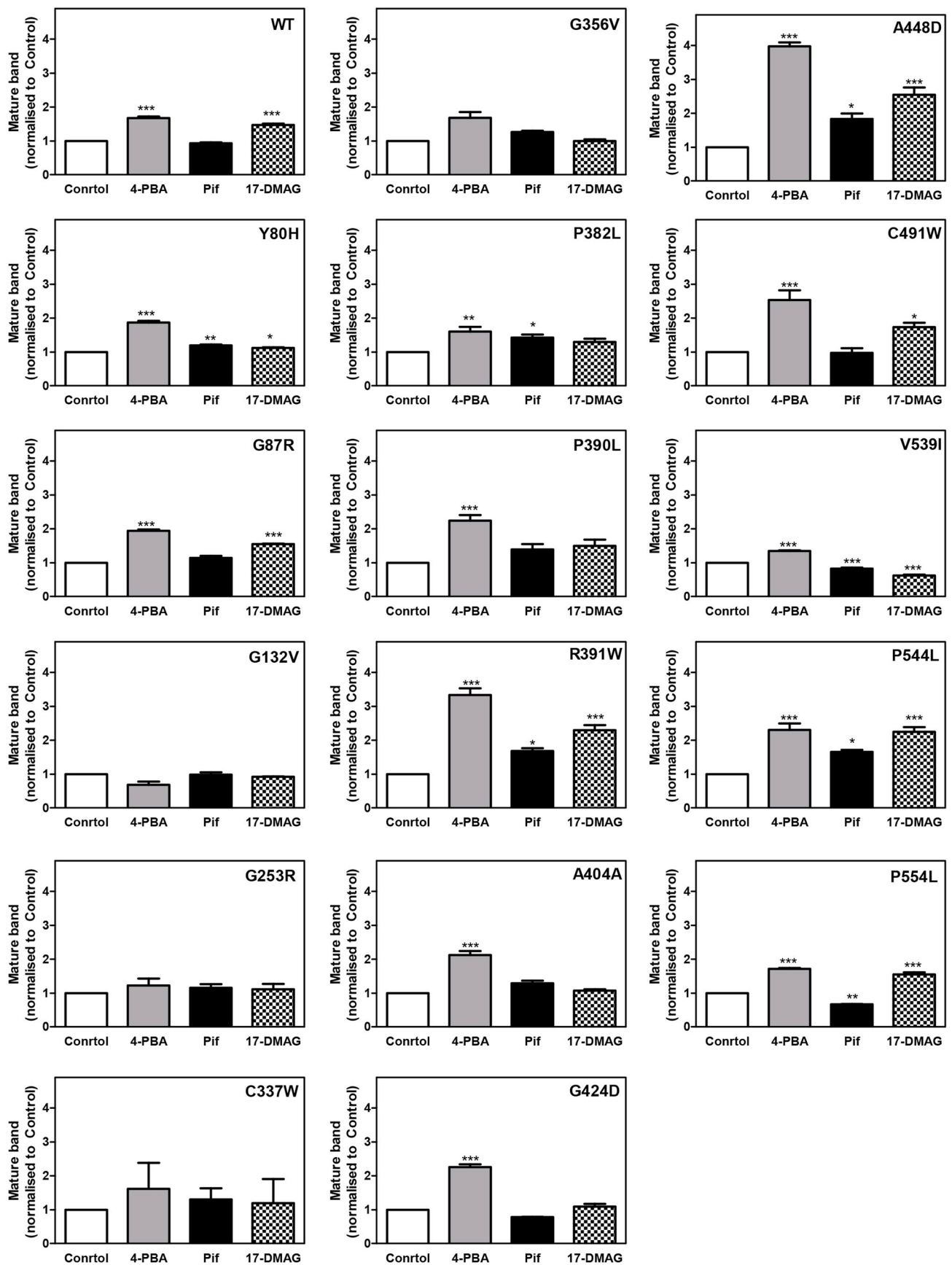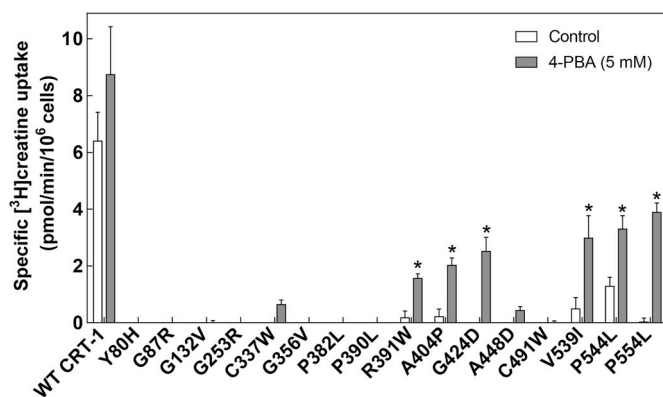
Fig. 4. (continued)

Fig. 5. Preincubation with 4-PBA restores - in part - uptake of [³H] creatine by HEK293 cells expressing CTD-causing mutants, hCRT-1-R391W, -404P, -G424D, -V539I, -P544L and –P554L. HEK293 cells expressing the wild type and mutant CRTs were treated for 24 h with 4-PBA (5 mM) and creatine uptake assays were performed as described in the legend to Fig. 1. Several mutants showed restored creatine uptake following the treatment. The data were obtained from three independent experiments, performed in triplicate. Error bars represent S.D.

(P544L) from TM11, which represents a separate domain in SLC6 transporters, *i.e.* it is not part of the inverted repeat. Two additional mutants, C337W and A448D, also show some degree of rescue by 4-PBA, albeit to a relatively modest extent of 5–10% of the wild type control (Fig. 5). Because of the micro-heterogeneity of hCRT1 (see Fig. 3), we verified by enzymatic digestion that the mature glycosylated was formed, for both the wild type protein and the mutants, in the presence of 4-PBA (Fig. 6). Only the wild type transporter and 4-PBA-responsive mutants (shown for hCRT-1-R391W, -A404P, -G424D and -P544L in Fig. 6) revealed mature glycosylated, endoglycosidase H-resistant species. In contrast, the Y80H variant, which was irresponsive to the action of 4-PBA (Fig. 5), contained predominantly the core-glycosylated, *i.e.* ER-resident transporter. We confirmed these data for two responsive mutants, hCRT-1-R391W and hCRT-1-P544L, by confocal microscopy: after 4-PBA treatment, the rescued mutants were found at the cell surface; the YFP-fluorescence co-localised with trypan blue fluorescence, which was used to delineate the plasma membrane (Fig. 7). Finally, we also examined the kinetics of creatine uptake for these two mutants prior to and after rescue with 5 mM 4-PBA (Fig. 8A–C). The treatment of HEK293 cells expressing the hCRT-1-R391W and -P544L with 4-PBA resulted in an approximately 3–4-fold increase in the maximum transport velocity V_{max} values (Table 1).

3.4. 4-PBA treatment promotes the distribution of hCRT-1-P544L, a CTD-inducing variant, into neurite extensions of isolated hippocampal neurons

CRT-1 is expressed in several brain areas including the hippocampus (Dodd et al., 2010); in hippocampal neurons, CRT-1 is delivered to both, dendrites and axons (Dodd et al., 2010). Accordingly, we compared the distribution of YFP-tagged wild type hCRT1 and hCRT1-P544L variant in hippocampal neurones: wild type hCRT1 was visualized throughout the arborisations of the neurite extensions and reached their distal tips (Fig. 9A). In contrast, the pathological variant hCRT1-P544L was confined to the neuronal soma and only entered the proximal segments of the neurites (Fig. 9B). However, if the neurones were incubated in the presence of 5 mM 4-PBA for 24 h, the distribution of hCRT1-P554L-YFP became similar to that of wild type hCRT1 (cf. Fig. 9C and A). We quantified these distributions by Sholl analysis (Fig. 9D, left hand panel) and calculated the area under the curve (AUC) for each individual neuron, which had been examined by confocal microscopy (Fig. 9D, right hand panel): these AUC-values differed in a statistically significant manner for neurons expressing wild type hCRT-1

and hCRT-1-P544L. In addition, the AUC-based analysis confirmed that 4-PBA enhanced the delivery of hCRT-1-P544L to the distal segments of the neurite extensions, such that its pattern resembled distribution of wild type hCRT-1.

4. Discussion

To the best of our knowledge we are the first to report that 4-PBA can effectively rescue the activity of several pathological hCRT-1 variants linked to CTD. 4-PBA is an approved drug, which is clinically used in the chronic management of urea cycle disorders in children, *i.e.* diseases caused by genetic defects in several enzymes involved in the urea cycle. Deficiency of these enzymes (*i.e.* carbamoyl phosphate synthetase I, ornithine transcarbamylase, argininosuccinate synthetase, argininosuccinate lyase, arginase I, citrin and ornithine translocase) leads to nitrogen waste build up in the blood plasma, forming ammonia glutamine. 4-PBA acts as a nitrogen-scavenger and assists kidneys in excreting excess ammonia from the body. Besides, 4-PBA is used for sickle cell disease due to its capacity to activate β-globin transcription (Dover et al., 1994; Qi et al., 2004) and is also under clinical investigation for use in cancer and Huntington's disease (Kolb et al., 2015). Moreover, the merits of 4-PBA in the therapy of cystic fibrosis are well renowned. Treatment with 4-PBA induces CFTR channel function in ΔF508-CFTR-expressing cystic fibrosis airway epithelial cells (Rubenstein and Zeitlin, 2000). This is achieved by 4-PBA stabilising the misfolded ΔF508-CFTR variant in the ER and allowing it to traffic to the cell membrane, though the mechanistic details underlying this effect happen to be more complex than initially presumed. We also observed that 4-PBA increased both, the ER-resident core glycosylated and the mature glycosylated species of wild type hCRT1 and of the responsive CTD mutants. This increase in total transporter levels does not per se argue against a chaperoning action of 4-PBA: the transporter must be first stabilised in the ER and subsequently exported. This is actually also seen with receptor ligands, which act as pharmacochaperone: in fact, in response to antagonists, a folding-deficient mutant of the A_1-adenosine receptors is stabilised and first accumulates in the ER, because it escapes ER-associated degradation (Kusek et al., 2015). Regrettably none of the misfolded DAT variants linked to infantile/juvenile parkinsonism and dystonia (Kurian et al., 2009; Ng et al., 2014) responded to 4-PBA treatment (Asjad et al., 2017). Surprisingly, the closely related serotonin transporter (SERT), showed marked increases in surface expression upon exposure to low mM concentrations of 4-PBA (Fujiwara et al., 2013). We further substantiated this finding for folding-deficient versions of SERT (El-Kasaby et al., 2014; Koban et al., 2015), which responded to 4-PBA treatment (El-Kasaby, Sucic and Freissmuth, unpublished data).

The precise mechanisms of action of 4-PBA are as yet ambiguous. Its capacity as a chemical chaperone has been thoroughly documented for the ABC transporter family in particular (Prulière-Escabasse et al., 2007; Iram and Cole, 2014; Gordo-Gilart et al., 2016; Pomozi et al., 2017). 4-PBA has been classified as a hydrophobic chaperone, which interacts with hydrophobic segments of unfolded proteins and protects them from aggregation. In addition, 4-PBA is known to reduce ER stress through molecular mechanisms, which apparently affect many levels of regulation. Some studies allude to synergistic actions of 4-PBA, such as *e.g.* downregulation or modulation of HSC70 expression (Rubenstein and Zeitlin, 2000), increase in HSP70 levels (possibly as a secondary effect of decreasing HSC70 levels), reversible histone deacetylase (HDAC) class I and IIa inhibition (Cousens et al., 1979; Konsoula and Barile, 2012), and signaling *via* Elp2 and STAT-3 (Suaud et al., 2011). 4-PBA-induced inhibition of HDACs leads to transcriptional regulation of genes in the unfolded protein response (UPR) system. This in turn induces the synthesis of molecular chaperones (HSPs) and downregulation of protein synthesis (Cortez and Sim, 2014). In fact, the neuroprotective effects of 4-PBA may be accounted to epigenetic regulators related to HDAC inhibition related to enhanced synaptic
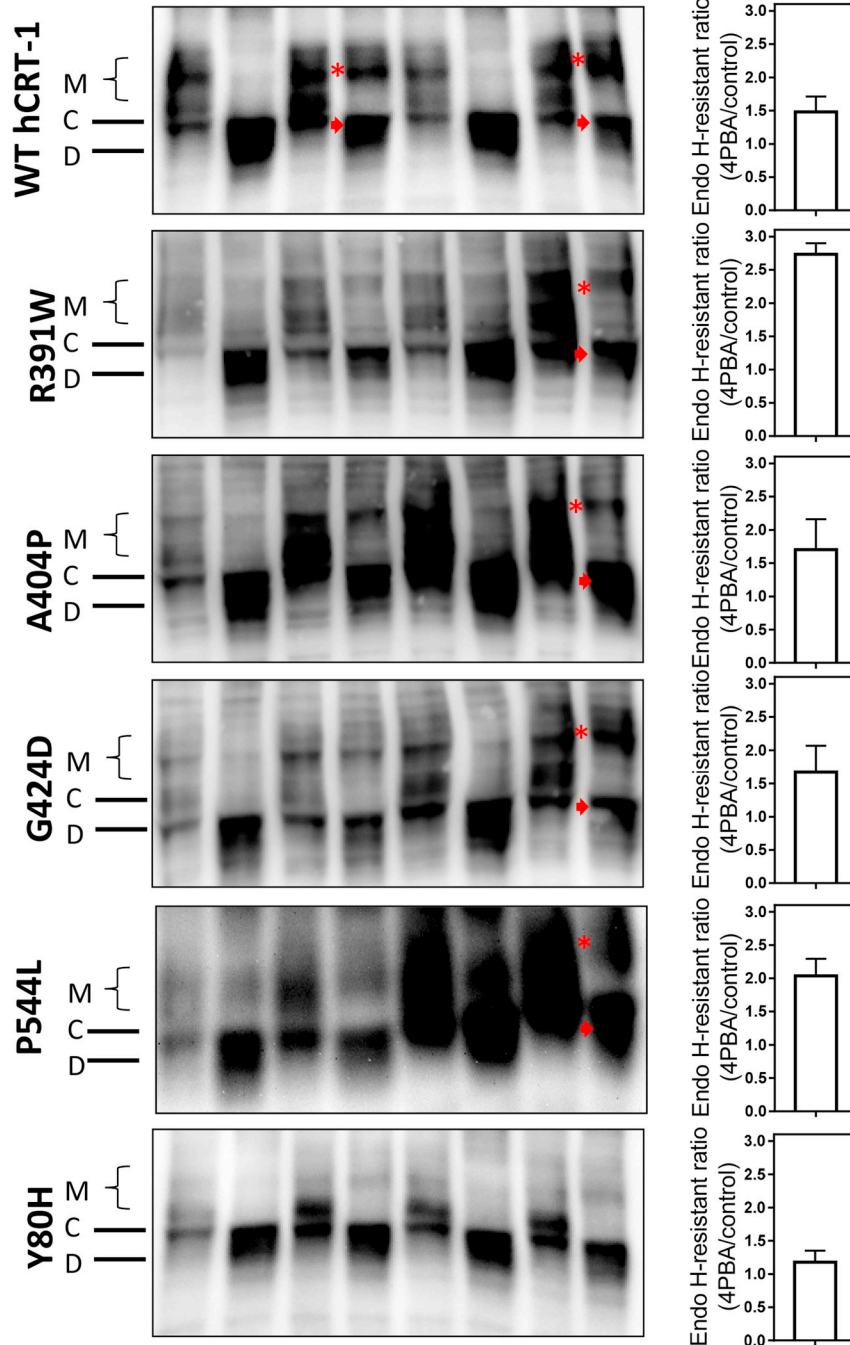
Fig. 6. Deglycosylation of wild type hCRT-1 and CTD variants in the presence of peptide-N-glycosidase F and endoglycosidase H. Detergent lysates were prepared from HEK293 cells transiently expressing WT hCRT-1-YFP and several CTD mutants thereof. Aliquots (20 μg) were diluted in the appropriate buffer and incubated in the absence (untreated controls, lanes 1 and 3; 4-PBA-treated, lanes 5 and 7) and presence of peptide-N-glycosidase F (1000 U, PNGase F, untreated control, lane 2 and 4-PBA-treated, lane 6) and of endoglycosidase H (1500 U, Endo H, untreated control, lane 4 and 4-PBA-treated, lane 8) for 2 h at 37 °C. The proteins were separated by electrophoresis, transferred to nitrocellulose and immunoreactivity visualized by immunoblotting with an anti-GFP antibody directed against the YFP-tag at the C-termini of the transporters. The red asterisk symbol marks the Endo H-resistant species of the mature glycosylated upper band (M). The red arrow denotes the Endo H-cleaved species of the lower core-glycosylated band (C). The ratios of endo H-resistant bands after 4-PBA treatment over corresponding controls were quantified using Image J. (For interpretation of the references to colour in this figure legend, the reader is referred to the Web version of this article.)

plasticity, learning and memory (Konsoula and Barile, 2012). Accordingly, 4-PBA showed beneficial effects in various cell culture and animal models of neurodegenerative disorders, *e.g.* Alzheimer's (Ricobaraza et al., 2009, 2012) and Parkinsons's disease (Inden et al., 2007; Ono, 2009).

It is worth mention that several pathological variants found in the hCRT-1 also trigger folding diseases at equivalent positions in other SLC6 family members. For instance, the replacement of glycine 132 by valine in hCRT-1 (*i.e* G132V-hCRT-1 variant) causes severe mental retardation in boys (Lion-François et al., 2006), and the mutation to glutamine of the equivalent glycine in *Drosophila melanogaster* DAT (*i.e.*

G108Q-dDAT), leads to a sleepless phenotype reminiscent of a DAT knock-out in flies (Kasture et al., 2016, 2017). Similarly, the mutation of P554 to leucine (L) elicits misfolding in both transporters and consequently leads to disease: infantile/juvenile parkinsonism-dystonia in hDAT (Kurian et al., 2009, 2011; Ng et al., 2014; Asjad et al., 2017), and severe mental retardation in hCRT-1 (Rosenberg et al., 2004, 2007; Mancini et al., 2005). The same holds true for the mutation to leucine (L) of P390 in hCRT-1 and the equivalent residue P395 in hDAT. P544 and P554 are located within TMD11 and the extracellular loop between TMDs 11 and 12, respectively. The proline residue P390-hDAT/P395-hCRT-1 is located in TMD8. At least seven CTD-causing hCRT-1
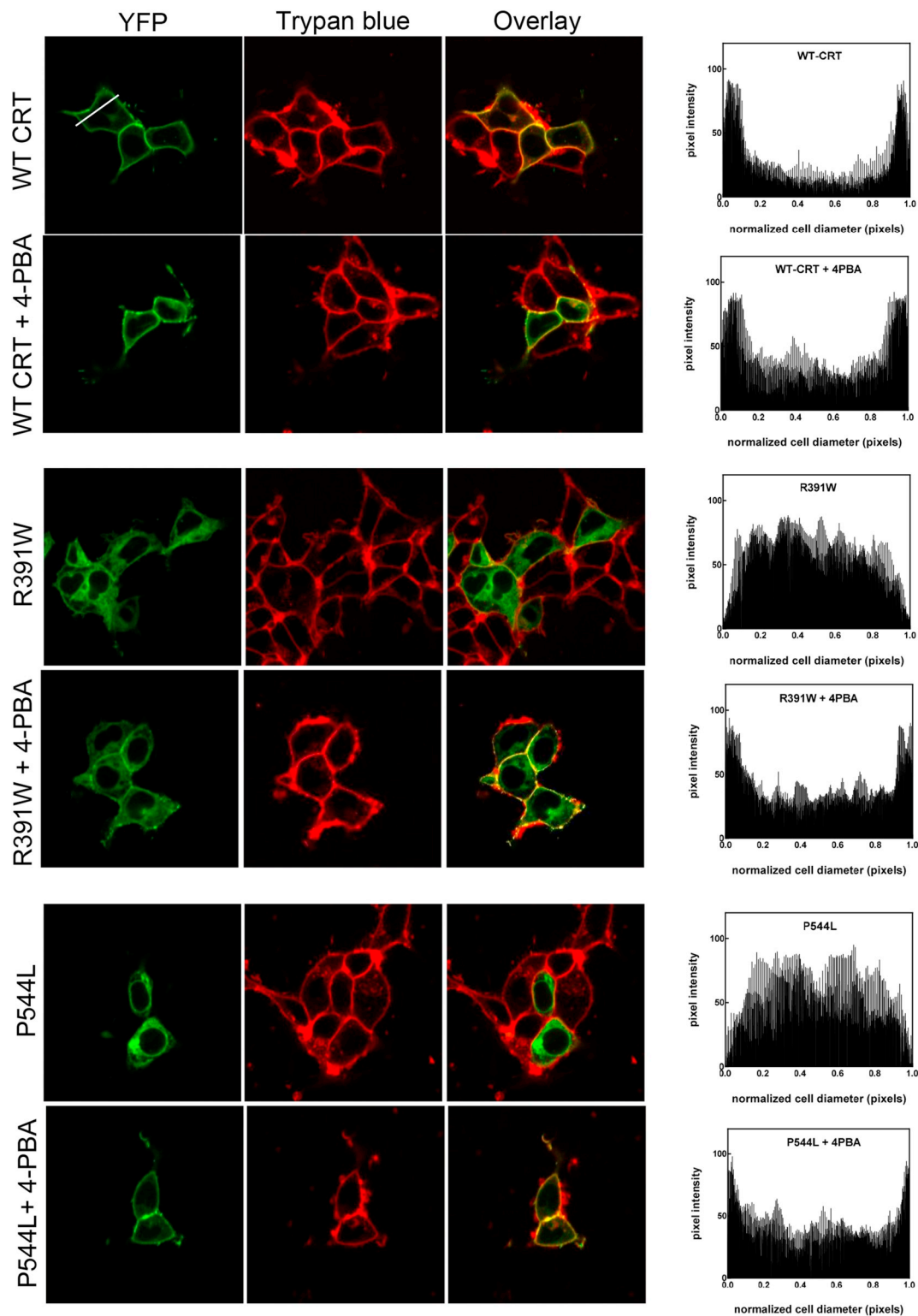
Fig. 7. Treatment with 4-PBA promotes the trafficking of CTD variants to the plasma membrane. HEK293 cells expressing the wild type and mutant CRTs were treated for 24 h with 4-PBA (5 mM). Confocal microscopy imaging of WT hCRT-1, hCRT-1-R391W and hCRT-1-P544L mutants was performed as described under *Material and Methods*. Cells exposed to 4-PBA are shown below the corresponding control (untreated) cells, for each of the transporters. Quantification of images, at least ten per condition, were carried out using the ImageJ software and the histograms are displayed as the rightmost panels. The white line in the top left panel, exemplifies the cross section of transfected cells used for the fluorescence analyses. The black area in the histogram corresponds to the mean fluorescence, the grey area represents the variation (S.D.).

mutations reported to date are substitutions of prolines by other residues, leucine being the most frequent substitution (*i.e.* P382L, P295R, P390L, P434L, P544L, P554L and P597T). Prolines are known to induce

kinks in proteins and their replacement by other residues is likely to perturb the protein structure, which in many instances accounts for folding defects. Proline is the only natural amino acid whose side chain
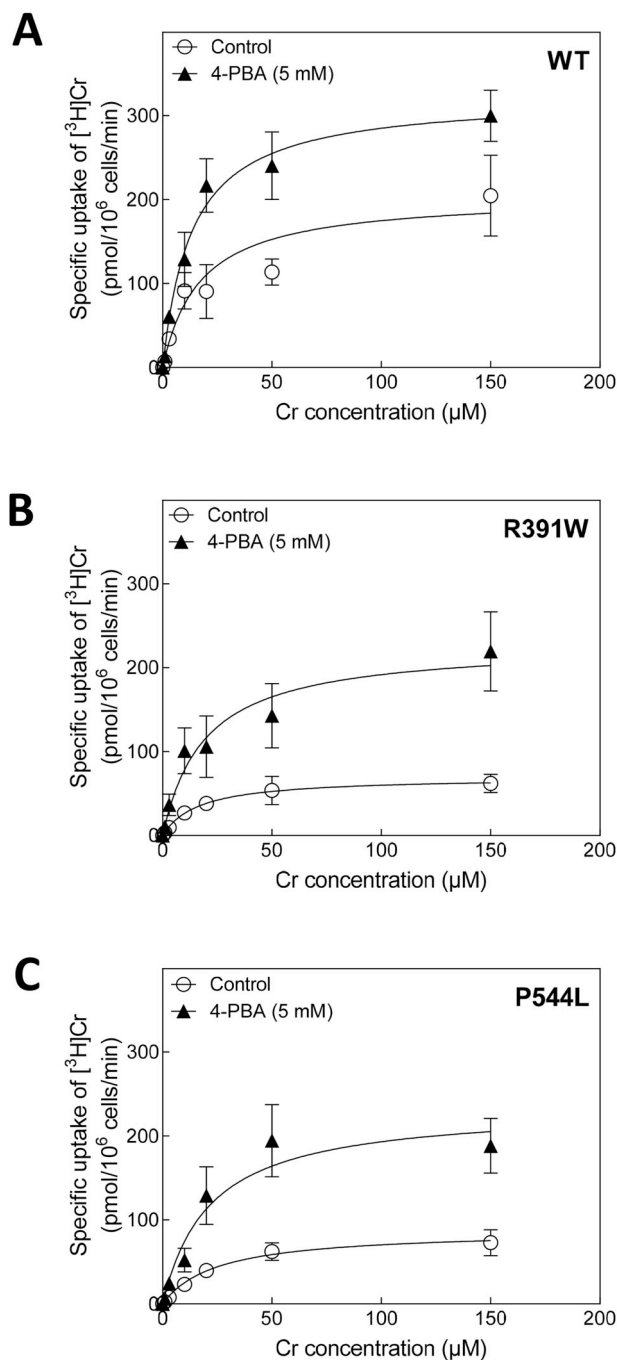
Fig. 8. Effects of 4-PBA on Michaelis-Menten kinetics of [³H] creatine uptake by wild type hCRT-1, hCRT-1-R391W and -P544L. Twenty four hours after transfection, HEK293 cells expressing the wild type hCRT-1 (A), R391W (B) and P544L (C) were incubated in the absence and presence of 4-PBA (5 mM) and seeded onto poly-D-lysine coated 48-well plates. [³H]Creatine uptake was determined by incubating the cells with uptake buffer containing 10 nM [³H] creatine, which was diluted with increased unlabeled creatine (in the final concentration range of 1–150 μM). The data were obtained from four independent experiments, in triplicates; the error bars indicate S.E.M.

Table 1

Creatine uptake kinetics by wild type hCRT-1 and two CTD variants before and after 4-PBA treatment. HEK293 cells were transiently transfected with plasmids encoding wild type hCRT-1 or two variants, R391W and P544L. 24 h later, cells were treated with or without 5 mM 4-PBA. Specific [³H]creatine uptake was measured 48 h after transfection (see *Material and Methods*).

hCRT-1	Control (untreated)		4-PBA-treated	
	K_M (μM)	V_{max} (pmol/ 10^6 cells/min)	K_M (μM)	V_{max} (pmol/ 10^6 cells/min)
WT	17.1 ± 6.6	204.7 ± 30.6	13.3 ± 4.6	322.9 ± 27.0 *
R391W	16.1 ± 5.9	69.8 ± 10.1	19.1 ± 9.7	228.2 ± 38.6 *
P544L	24.7 ± 8.2	87.7 ± 10.7	21.5 ± 8.0	234.5 ± 29.9 *

The K_M and V_{max} values were calculated from data shown in Fig. 8. The values are represented as arithmetic means ± S.E.M. from four independent experiments, performed in triplicate. V_{max} values of the untreated versus 4-PBA-treated cells were statistically different for the two CTD variants (*, P < 0.05, paired t tests).

delay, hyperactivity and abnormal behaviour, as well as myoclonic seizures (Mencarelli et al., 2011). Another CTD variant associated with epilepsy is hCRT1-P544; it is manifested by moderate mental retardation, delayed language and motor development, but accompanied by multifocal epileptic waves (Mancini et al., 2005; Betsalel et al., 2012). The P554L variant leads to hypotonia, severe intellectual disability and drug-resistant epilepsy, and sudden death of one patient at the age of 17 (Rosenberg et al., 2004; Nozaki et al., 2015). One clinical study reported significantly higher levels of guanidinoacetic acid (GAA) in the brains of CTD patients, with creatine being virtually absent (Sijens et al., 2005). CRT-1 is known to play a role in the transport of GAA in the brain and the blood cerebrospinal fluid barrier, albeit with a K_M value 10-fold greater than that of creatine (Tachikawa et al., 2008). The lack of functional CRTs in CTD leads to cerebral accumulation of GAA. Because GAA is an endogenous convulsant, this may account for at least some of the epileptic seizures observed in many CTD patients. At this point, none of the currently available therapeutic interventions can ameliorate the clinical outcome in any of the diagnosed CTD patients. One likely rationalisation for this is that creatine is released from central neurons and exerts its action as a neuromodulator (Almeida et al. 2006). In effect, hCRT-1 must play a major role in taking up the previously released creatine (Peral et al. 2010) and/or releasing creatine from neurons (Mak et al. 2009). Consequently, even though supplementation with creatine itself might improve creatine levels, it cannot compensate for the neuromodulatory action accomplished by the plasmalemmal hCRT-1. We hence postulate that in CTD, hCRT-1 is absent from its physiological site of action in neuronal cells. The localization of hCRT-1 in the human brain was mapped out using immunohistochemistry: the transporter is robustly expressed in the large projection neurones of the brain and spinal cord (*i.e* in the pyramidal neurones in the cerebral cortex, Purkinje cells in the cerebellar cortex and motor neurones of the somatic motor and visceromotor cranial nerve nuclei and the ventral horn of the spinal cord), while only negligible levels of CRT-1 were mapped to substantia nigra and locus coeruleus, *i.e.* regions typically implicated in neurodegenerative diseases (Lowe et al., 2015). The absence of functional CRTs in brain cells portends that the energy normally conferred by creatine is no longer attainable, since creatine is taken up and/or released from these cells *via* membrane-bound CRTs. Since many CTD-triggering variants of hCRT-1 are confined to the ER due to protein folding defects, 4-PBA treatment may be the key to tackling CTD, by rectifying their folding, trafficking and transport activity. Proper trafficking, *e.g.* axonal targeting of SERT in rat dorsal raphe neurons is specified by SEC24C-dependent ER export (Montgomery et al., 2014). SERT mutants, which are either folding-deficient or harbour a disrupted SEC24C-recognition motif are also trapped in the ER (Sucic et al., 2011, 2013). The same holds true for misfolded variants of hDAT associated with infantile

connects to the protein backbone twice, forming a five-membered nitrogen-containing ring. The main chain conformations that can be adopted by prolines are hence limited in comparison to any other amino acid.

On a clinical level, CTD encompasses a vast range of symptoms contingent on the particular variant. Some mutations elicit much graver phenotypes than others. The R391W variant is accompanied by speech
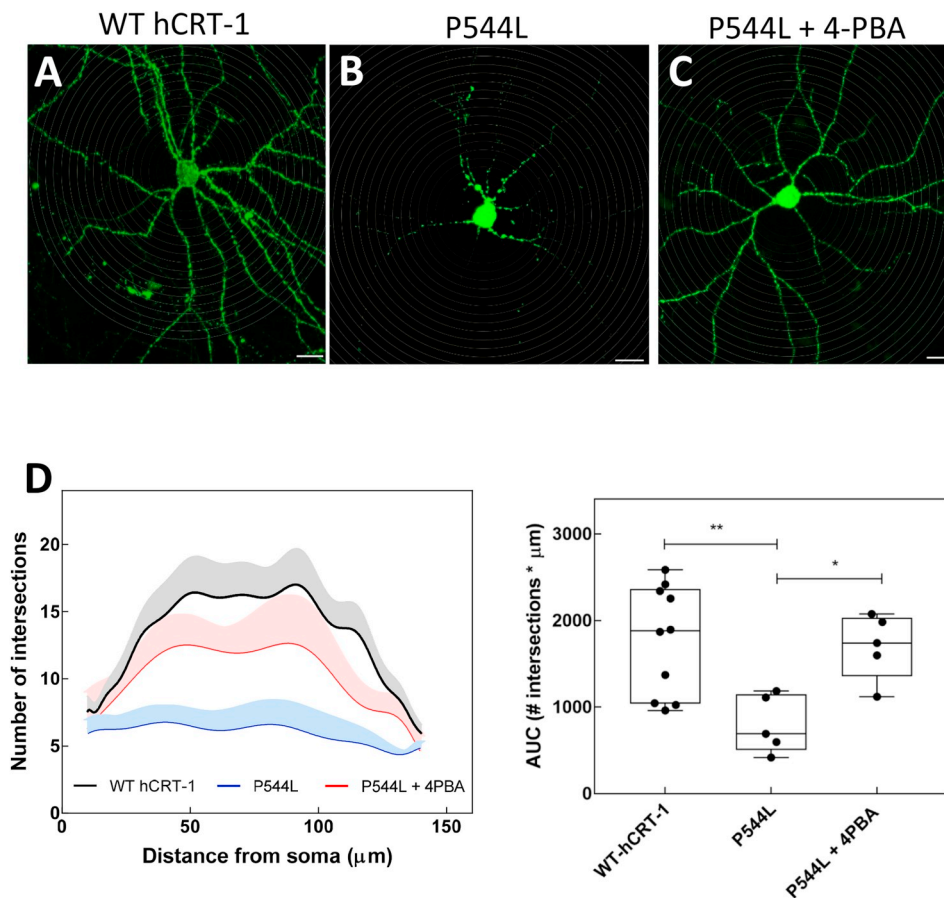
Fig. 9. Distribution of hCRT-1 and hCRT-1-P544L in hippocampal neurons. Panels (A) to (C) show confocal images of hippocampal neurons expressing wild type hCRT-1-YFP (A, n = 10) and the CTD-causing variant hCRT-1-P544L (B, n = 5 and C, n = 5). Primary hippocampal neurons were transiently transfected with plasmids expressing wild type hCRT-1 and –P544L, 48 h prior to imaging. In Panel (C), neurons were incubated with 5 mM 4-PBA for 24 h prior to imaging (scale bar = 20 μm). Panel (D) shows quantitative analysis of the neuron images, performed using Sholl analysis with radii increasing in 2 μm increments as indicated by the dotted circles; the shaded area indicates the variation (S.E.M.) for the intersections at individual radii. In the bottom right-hand panel, the area under the curve (AUC) was calculated for individual neuron summarized in panel (D). The box plot shows the median and the interquartile range, whiskers indicate minimum and maximum values. The statistical comparison was done by a Kruskal-Wallis test followed by Dunn's multiple comparison (*: P < 0.05, **: P < 0.01).

Parkinsonism/dystonia; several of which were functionally rescued by pharmacochaperoning, both in HEK293 cells and in living flies (Kasture et al., 2016; Asjad et al., 2017).

Several groups studied CTD mouse models, which largely mimicked the symptoms (*i.e.* impaired cognition and autistic-like behaviour) of the human disease (Kurosawa et al., 2012; Baroncelli et al., 2016; Stockebrand, 2018). The CRT-1 knockout mice showed a drastic deterioration in the GABAergic system, reduced hippocampal neurogenesis, prominent activation of microglia and altered oxidative metabolism (Baroncelli et al., 2016). This explains some of the epilepsy symptoms experienced by many CTD patients. To date, only Kurosawa and co-workers explored the possible therapeutic options for managing CTD, showing that, in contrast to creatine itself, its analogue cyclocreatine enhanced cognitive abilities in mice with a brain-specific CRT-1 knockout (Kurosawa et al., 2012). Our data suggest that 4-PBA may be an effective strategy for treating CTD. 4-PBA is administered in doses of up to 20 g/d and 0.5 g/kg/d for adults and children < 20 kg, respectively. Therapeutic doses translate into plasma concentrations ≥1 mM. Thus, it may be justified to test 4-PBA in patients harbouring those mutations, which we found to be responsive when expressed in HEK293 cells. More importantly, our work provides a proof-of-principle that the folding deficiency of mutant hCRT-1 variants is amenable to pharmacological correction. This justifies the search for additional and possibly improved pharmacochaperones.

Conflicts of interest

The authors declare no conflicts of interest.

Funding

This work was supported by the Austrian Science Fund (project

References

Almeida, L.S., et al., 2006. Exocytotic release of creatine in rat brain. Synapse 60, 118–123.

Ardon, O., et al., 2016. Creatine transporter deficiency: novel mutations and functional studies. Mol. Genet. Metab. Rep. 8, 20–23.

Asjad, H.H.M., et al., 2017. Pharmacochaperoning in a drosophila model system rescues human dopamine transporter variants associated with infantile/juvenile parkinsonism. J. Biol. Chem. 292, 19250–19265.

Baroncelli, L., et al., 2016. A mouse model for creatine transporter deficiency reveals early onset cognitive impairment and neuropathology associated with brain aging. Hum. Mol. Genet. 25, 4186–4200.

Betsalel, O.T., et al., 2012. Creatine Transporter Research, Group, Jakobs C, Salomons GS. Detection of variants in SLC6A8 and functional analysis of unclassified missense variants. Mol. Genet. Metabol. 105, 596–601.

Christie, D.L., 2007. Functional insights into the creatine transporter. In: Salomons, G.S., Wyss, M. (Eds.), Creatine and Creatine Kinase in Health and Disease. Springer, pp. 99–118.

Costes, S.V., et al., 2004. Automatic and quantitative measurement of protein-protein colocalization in live cells. Biophys. J. 86, 3993–4003.

Cousens, L.S., Gallwitz, D., Alberts, B.M., 1979. Different accessibilities in chromatin to histone acetylase. J. Biol. Chem. 254, 1716–1723.

DesRoches, C.L., et al., 2015. Estimated carrier frequency of creatine transporter deficiency in females in the general population using functional characterization of novel missense variants in the SLC6A8 gene. Gene 565, 187–191.

Dodd, J.R., et al., 2010. Functional and immunocytochemical characterization of the creatine transporter in rat hippocampal neurons. J. Neurochem. 115, 684–693.

Dover, G.J., Brusilow, S., Charache, S., 1994. Induction of fetal hemoglobin production in subjects with sickle cell anemia by oral sodium phenylbutyrate. Blood 84, 339–343.

El-Kasaby, A., et al., 2014. A cytosolic relay of heat shock proteins HSP70-1A and HSP90β

monitors the folding trajectory of the serotonin transporter. J. Biol. Chem. 289, 28987–29000.

Freissmuth, M., Stockner, T., Sucic, S., 2018. SLC6 transporter folding diseases and pharmacochaperoning. In: Handbook of Experimental Pharmacology: Targetting Trafficking in Drug Development. Springer, pp. 249–270 (Chapter 4).

Fujiwara, M., et al., 2013. Effects of the chemical chaperone 4-phenylbutylate on the function of the serotonin transporter (SERT) expressed in COS-7 cells. J. Pharmacol. Sci. 122, 71–83.

Geier, P., et al., 2011. Dynamic interplay of excitatory and inhibitory coupling modes of neuronal L-type calcium channels. Am. J. Physiol. Cell Physiol. 300, C937–C949.

Gordo-Gilart, R., et al., 2016. Functional rescue of trafficking-impaired ABCB4 mutants by chemical chaperones. PLoS One 11, e0150098.

Hahn, K.A., 2002. X-linked mental retardation with seizures and carrier manifestations is caused by a mutation in the creatine-transporter gene (SLC6A8) located in Xq28. Am. J. Hum. Genet. 70, 1349–1356.

Heussinger, N., et al., 2017. Variable white matter atrophy and intellectual development in a family with X-linked creatine transporter deficiency despite genotypic homogeneity. Pediatr. Neurol. 67, 45–52.

Hohenegger, M., et al., 1996. Thiophosphorylation of the G protein β-subunit in human platelet membranes: evidence against a direct phosphate transfer reaction to Gα subunits. Mol. Pharmacol. 49, 73–80.

Inden, M., et al., 2007. Neurodegeneration of mouse nigrostriatal dopaminergic system induced by repeated oral administration of rotenone is prevented by 4-phenylbutyrate, a chemical chaperone. J. Neurochem. 101, 491–1504.

Iram, S.H., Cole, S.P., 2014. Differential functional rescue of Lys(513) and Lys(516) processing mutants of MRP1 (ABCC1) by chemical chaperones reveals different domain-domain interactions of the transporter. Biochim. Biophys. Acta 1838, 756–765.

Kasture, A., et al., 2016. Functional rescue of a misfolded Drosophila melanogaster dopamine transporter mutant associated with a sleepless phenotype by pharmacological chaperones. J. Biol. Chem. 291, 20876–20890.

Kasture, A., et al., 2017. An unfolding story: small molecules remedy misfolded monoamine transporters. Int. J. Biochem. Cell Biol. 92, 1–5.

Koban, F., et al., 2015. A salt bridge linking the first intracellular loop with the C terminus facilitates the folding of the serotonin transporter. J. Biol. Chem. 290, 13263–13278.

Kolb, P.S., et al., 2015. The therapeutic effects of 4-phenylbutyric acid in maintaining proteostasis. Int. J. Biochem. Cell Biol. 61, 45–52.

Konsoula, Z., Barile, F.A., 2012. Epigenetic histone acetylation and deacetylation mechanisms in experimental models of neurodegenerative disorders. J. Pharmacol. Toxicol. Methods 66, 215–220.

Kurian, M.A., et al., 2009. Homozygous loss-of-function mutations in the gene encoding the dopamine transporter are associated with infantile parkinsonism-dystonia. J. Clin. Investig. 119, 1595–1603.

Kurian, M.A., et al., 2011. Clinical and molecular characterisation of hereditary dopamine transporter deficiency syndrome: an observational cohort and experimental study. Lancet Neurol. 10, 54–62.

Kurosawa, Y., et al., 2012. Cyclocreatine treatment improves cognition in mice with creatine transporter deficiency. J. Clin. Investig. 122, 2837–2846.

Kusek, J., et al., 2015. Chaperoning of the A1-adenosine receptor by endogenous adenosine - an extension of the retaliatory metabolite concept. Mol. Pharmacol. 87, 39–51.

Lion-François, L., et al., 2006. High frequency of creatine deficiency syndromes in patients with unexplained mental retardation. Neurology 67, 1713–1714.

Lowe, M.T., et al., 2015. Distribution of the creatine transporter throughout the human brain reveals a spectrum of creatine transporter immunoreactivity. J. Comp. Neurol. 523, 699–725.

Mak, C.S., et al., 2009. Immunohistochemical localisation of the creatine transporter in the rat brain. Neuroscience 163, 571–585.

Mancini, G.M., et al., 2005. Two novel mutations in SLC6A8 cause creatine transporter defect and distinctive X-linked mental retardation in two unrelated Dutch families. Am. J. Med. Genet. 132A, 288–295.

Mencarelli, M.A., et al., 2011. Creatine transporter defect diagnosed by proton NMR spectroscopy in males with intellectual disability. Am. J. Med. Genet. 155A, 2446–2452.

Montgomery, T.R., et al., 2014. Axonal targeting of the serotonin transporter in cultured rat dorsal raphe neurons is specified by SEC24C-dependent export from the endoplasmic reticulum. J. Neurosci. 34, 6344–6351.

Ng, J., et al., 2014. Dopamine transporter deficiency syndrome: phenotypic spectrum from infancy to adulthood. Brain 137, 1107–1119.

Nozaki, F., et al., 2015. A family with creatine transporter deficiency diagnosed with urinary creatine/creatinine ratio and the family history: the third Japanese familial case. No Hattatsu 47, 49–52.

Ono, K., 2009. A chemical chaperone, sodium 4-phenylbutyric acid, attenuates the pathogenic potency in human alpha-synuclein A30P + A53T transgenic mice. Park. Relat. Disord. 15, 649–654.

Peral, M.J., Vázquez-Carretero, M.D., Ilundain, A.A., 2010. Na(+)/Cl(-)/creatine transporter activity and expression in rat brain synaptosomes. Neuroscience 165, 53–60.

Pomozi, V., et al., 2017. Functional rescue of ABCC6 deficiency by 4-phenylbutyrate therapy reduces dystrophic calcification in Abcc6-/- mice. J. Investig. Dermatol. 137, 595–602.

Prulière-Escabasse, V., et al., 2007. Modulation of epithelial sodium channel trafficking and function by sodium 4-phenylbutyrate in human nasal epithelial cells. J. Biol. Chem. 282, 34048–34057.

Qi, X., et al., 2004. Sodium 4-phenylbutyrate protects against cerebral ischemic injury. Mol. Pharmacol. 66, 899–908.

Ricobaraza, A., et al., 2009. Phenylbutyrate ameliorates cognitive deficit and reduces tau pathology in an Alzheimer's disease mouse model. Neuropsychopharmacology 34, 1721–1732.

Ricobaraza, A., et al., 2012. Phenylbutyrate rescues dendritic spine loss associated with memory deficits in a mouse model of Alzheimer disease. Hippocampus 22, 1040–1050.

Rosenberg, E.H., et al., 2004. High prevalence of SLC6A8 deficiency in X-linked mental retardation. Am. J. Hum. Genet. 75, 97–105.

Rosenberg, E.H., et al., 2007. Functional characterization of missense variants in the creatine transporter gene (SLC6A8): improved diagnostic application. Hum. Mutat. 28, 890–896.

Rubenstein, R.C., Zeitlin, P.L., 2000. Sodium 4-phenylbutyrate downregulates Hsc70: implications for intracellular trafficking of DeltaF508-CFTR. Am. J. Physiol. Cell Physiol. 278, C259–C267.

Sijens, P.E., et al., 2005. 1H MR spectroscopy of the brain in Cr transporter defect. Mol. Genet. Metabol. 86, 421–422.

Steentoft, C., et al., 2013. Precision mapping of the human O-GalNAc glycoproteome through SimpleCell technology. EMBO J. 32, 1478–1488.

Straumann, N., et al., 2006. Effects of N-linked glycosylation on the creatine transporter. Biochem. J. 393, 459–469.

Suaud, L., et al., 2011. 4-Phenylbutyrate stimulates Hsp70 expression through the Elp2 component of elongator and STAT-3 in cystic fibrosis epithelial cells. J. Biol. Chem. 286, 45083–45092.

Sucic, S., et al., 2010. The N terminus of monoamine transporters is a lever required for the action of amphetamines. J. Biol. Chem. 285, 10924–10938.

Sucic, S., et al., 2011. The serotonin transporter is an exclusive client of the coat protein complex II (COPII) component SEC24C. J. Biol. Chem. 286, 16482–16490.

Sucic, S., et al., 2013. Switching the clientele: a lysine residing in the C terminus of the serotonin transporter specifies its preference for the coat protein complex II component SEC24C. J. Biol. Chem. 288, 5330–5341.

Stockebrand, M., 2018. A mouse model of creatine transporter deficiency reveals impaired motor function and muscle energy metabolism. Front. Physiol. 9, 773.

Tachikawa, M., et al., 2008. Expression and possible role of creatine transporter in the brain and at the blood-cerebrospinal fluid barrier as a transporting protein of guanidinoacetate, an endogenous convulsant. J. Neurochem. 107, 768–778.

Uemura, T., et al., 2017. Abnormal N-glycosylation of a novel missense creatine transporter mutant, G561R, associated with cerebral creatine deficiency syndromes alters transporter activity and localization. Biol. Pharm. Bull. 40, 49–55.

van de Kamp, J.M., et al., 2012. Long-term follow-up and treatment in nine boys with X-linked creatine transporter defect. J. Inherit. Metab. Dis. 35, 141–149.

van de Kamp, J.M., et al., 2013. Phenotype and genotype in 101 males with X-linked creatine *transporter deficiency*. J. Med. Genet. 50, 463–472.

The abbreviations used are

4-PBA: 4-phenylbutyrate
CRT-1: creatine transporter 1
hCRT-1: human CRT-1
DAT: dopamine transporter
dDAT and hDAT: drosophila and human DAT
Endo H: endoglycosidase H
ER: endoplasmic reticulum
CFP: cyan fluorescent protein
HEK293: human embryonic kidney 293
HSP: heat shock protein
PBS: phosphate-buffered saline
SERT: serotonin transporter
TBS: Tris-buffered saline
PNGase F: peptide-N-glycosidase F
SLC6: solute carrier 6
YFP: yellow fluorescent protein